

This is the accepted manuscript made available via CHORUS. The article has been published as:

Large artificial anisotropic growth rate in on-lattice simulation of obliquely deposited nanostructures

B. Tanto, C. F. Doiron, and T.-M. Lu

Phys. Rev. E **83**, 016703 — Published 28 January 2011

DOI: [10.1103/PhysRevE.83.016703](https://doi.org/10.1103/PhysRevE.83.016703)

Large artificial anisotropic growth rate in on-lattice simulation of obliquely deposited nanostructures

B. Tanto^{a)}, C. F. Doiron, T. –M. Lu

Center for Integrated Electronics, and

Department of Physics, Applied Physics, and Astronomy,

Rensselaer Polytechnic Institute, Troy, New York 12180, USA

Abstract

On-lattice particle simulation is one of the most common types of Monte Carlo simulations used in studying the dynamics of film growth. We report the observation of a large artificial anisotropic growth rate variation due to the fixed arrangement of particles in an on-lattice simulation of oblique angle deposition (OAD). This unexpectedly large anisotropy is not reported in previous literatures and substantially affects the simulation outcomes such as column angle and porosity, two of the most essential quantities in obliquely deposited nanostructures. The result of our finding is of interest to all on-lattice simulations in obliquely deposited films/nanostructures.

PACS number(s): 68.55.J-, 05.10.Ln, 81.07.-b, 81.15.Aa

Keywords: on-lattice simulation, oblique angle deposition, glancing angle deposition, sculptured thin film, Monte Carlo, column angle, fan angle

^{a)} Electronic mail: boy.tanto@gmail.com

INTRODUCTION

Microstructure of thin films is of great interest from both scientific and practical point of views^{1,2}. Using statistical physics and fractal concepts, it has been possible to quantify and predict the morphology and microstructure of seemingly random phenomena of films growth, such as the evolution of surface roughness of a film. Computer simulation is often used in aiding the advancement in this field of study. In particular, OAD has emerged in recent years as an increasingly important fabrication technique due to its ability to create unique and useful film microstructure^{3,4}. OAD can be used to tune the porosity of a given material easily, cost-effectively, continuously, and over a wide range of values^{3,4}. Porosity of a material is directly related to its physical properties such as: index of refraction, dielectric constant, thermal conductivity, resistivity, and stiffness. Besides porosity tuning, another highly attractive feature of OAD is its ability to easily create large array of complex nanostructures that cannot be practically fabricated using other techniques. Some examples are: array of helical nanosprings and chevron structures⁴.

Despite the increasing popularity of OAD, predicting the outcome of obliquely deposited nanostructure is still a challenging problem⁵⁻⁷. Monte Carlo simulation is a very attractive method of studying OAD because it offers unique insight into OAD. It is also useful for predicting outcome of an experiment. Simulation has been able to match geometry of nanostructures and morphology of film fabricated using OAD⁸. Simulation has also been a very valuable tool to study the growth dynamics of OAD films^{9,10}.

The most popular simulation approach uses discrete particles because it is relatively simple to construct and it mimics the behavior of particles during OAD. Shadowing and overhanging structures, two of the most crucial features in OAD, are straightforward to implement in particle simulation. These features are difficult to implement accurately in some other approaches (example: continuum approach¹¹).

Particle simulations can be categorized into two types: off-lattice and on-lattice simulation. The on-lattice simulation is popular due to its simplicity and its low usage of computing resources. Low usage of computing resources is not a small advantage because simulation using larger number of particles increases the accuracy of the simulation and in some cases is a necessity (e.g. for growth evolution of thick film). Various versions of on-lattice simulation of OAD has been developed and used by different research groups^{9,12-22}.

Unfortunately, on-lattice simulation requires arranging the impinging particles according to the lattice (grid) system implemented in the simulation. This lattice or grid orientation has nothing to do with the actual orientation of atoms in the real life experiment, which can present important yet non-obvious problems as we will describe in this paper.

In this work, we present our finding of how an on-lattice simulation in OAD can give highly anomalous and unrealistic results. Despite the wide use of computer simulation in OAD, and despite on-lattice particle simulation being the most common type of simulation, such a large artificial effect has not been reported before in literatures. We discuss why and how this grid effect affects the outcome of OAD simulation. We also propose practical ways to detect the presence of grid effect in a simulation.

EXPERIMENT AND SIMULATION

Imagine performing deposition on a floating seed (i.e. a seed without an underlying plane of substrate, see the schematic diagram in Fig. 1). This deposition yields fan structures^{7,8}. For a perfectly symmetrical seed, deposition from any direction must yield fans of the same shape and size. If the seed is not perfectly symmetrical, deposition from different directions will not yield fans of the exact same shape and size. However, for fan dimensions several times larger than the seed size, it is expected that the initial seed geometry does not affect the final outcome much, and thus the fans deposited from various

directions should be similar in size and shape if the deposition is long enough (as shown schematically in Fig. 1).

Figure 2 shows experimental results of deposition onto pillar seeds from two different flux angles. It can be seen that the fan angles ϕ are very close to each other, which confirms our expectation. The deposited material is Si at 0.8 nm/s flux rate using ebeam thermal evaporation with chamber base pressure at 5×10^{-7} Torr. The distance from source to substrate is about 40 cm. The seeds are UV curable Polyset nanoimprinted structures²³ on Si substrate. The substrate is at ambient chamber temperature (25 – 45° C) during deposition.

Figure 3 shows an on-lattice simulation of depositions on line seeds from various directions perpendicular to the line seeds (the length of the line is into the page). The three-dimensional (3D) Monte Carlo (MC) simulation we use in this paper is based on cubic particles that move and rest in simple cubic lattice configuration. Incoming particles are initiated at random locations above the substrate with uniform distribution and move towards the substrate in a straight line. An incoming particle sticks to existing deposited particles if it moves into one of their nearest neighbor locations. Surface diffusion is achieved by allowing translation of one randomly chosen particle (can be the incoming particle itself) located within a certain distance from the incoming particle. The diffusion is repeated D number of times. The translation of the particle is allowed if it increases its number of nearest neighbors. Periodic boundary condition is implemented on all the vertical walls of the simulation. More detailed explanation of the simulation is available in ref. 9. Figure 3 is obtained by running six simulations separately, each of size $512 \times 512 \times 512$, and each result displayed is a stitched image of two side by side simulation outputs (resulting in 512×1024 display).

As can be seen in Fig. 3, the result of the simulation deviates severely from expectation and certainly is not a small effect that can be ignored. As pointed out in our recent paper, the fan angle is directly related to the column angle of the columnar structures obtained by OAD⁷. The relationship

between fan angle and column angle is $\beta = \alpha - \phi/2$ for highly oblique deposition angle ($\alpha > \phi$). Both the column angle and the deposition angle are defined with respect to the substrate normal.

The much smaller fan angle shown in Fig. 3 for 45° deposition is due to the growth rate difference between the 0° and 45° depositions. This growth rate can be explained by an approximate analysis of the landing of the individual particles. As shown in Fig. 4(b), there are two types of growth for the 0° impinging particle. Each landing site results in its own growth thickness and direction. For 0° deposition the growth perpendicular and parallel to the flux are both $1a$, where a is the dimension of the cube. The resultant growth thickness is therefore $\sqrt{2}a$, and the direction is at 45° with respect to the flux. A two-dimensional seed has two opposite sides for growth perpendicular to the flux (i.e. the left and right side), each side with 45° growth with respect to the flux direction. This makes a fan angle of $45^\circ \times 2 = 90^\circ$. This estimated result is close to the fan angle obtained from simulation ($\sim 100^\circ$, Fig. 6).

For the 45° incident flux, the resultant growth thickness can be obtained by vector addition of the two possible growth mechanisms as shown in Fig. 4(d). The resultant growth thickness is $\sqrt{5}a$ (see Appendix). The angle between the resultant growth direction and the incoming flux is 18.4° (see Appendix). Using similar argument as before, the expected fan angle is therefore $2 \times 18.4^\circ = 36.8^\circ$, also close to the simulation result ($\sim 35^\circ$, Fig. 6). The resultant growth thickness for 45° deposition is larger than the thickness for 0° deposition even though the mass of deposited material is the same. Therefore, the 45° deposition results in higher porosity structures and smaller fan angle.

The degree of grid effect can be reduced by increasing the diffusion of the particles. Grid effect is caused by the large anisotropic growth rates. Diffusion reduces grid effect because diffusion is non-directional and thus smoothens out the anisotropy. The fan structures obtained by MC simulation using $D = 100$ is shown in Fig. 5. The plot of the fan angles obtained at various deposition angles is shown in Fig. 6. The figure shows that for higher diffusion, the difference in ϕ angle for 0° and 45° deposition is reduced from $\sim 50^\circ$ to $\sim 38^\circ$.

Fig. 3 and Fig. 5 enable quantification of the amount of grid effect on fan angle. Since fan angle is related to column angle in a known way⁷, the amount of influence of grid effect on column angle simulation can be calculated based on the data from Fig. 3 and Fig. 5. However, the relationships between fan angle and other physical quantities (such as porosity) are not yet available. Therefore, although Fig. 3 and Fig. 5 are useful in showing the presence of grid effect in a simulation, they do not necessarily provide an estimate of the amount of grid effect in quantities other than fan angle. We propose that an estimation of the amount of grid effect on any given quantity of interest can be obtained by comparing simulation outcomes from a normal setup and a “rotated setup”. The “rotated setup” is a setup whereby the source and the substrate are rotated together with respect to the simulation lattice (or, an equivalent point of view is that the lattice is rotated while fixing the substrate and source). The rotation is done in such a way that the source to substrate relative orientation and distance remains the same. The rotation angle is chosen so that the largest amount of grid effect is expected, based on Fig. 3. As an example, we performed the following simulations.

We created a substrate that consists of seeded and unseeded area to enable the observation of columnar angles on both seeded and unseeded surfaces. We deposit particles onto the seed at various flux angles α (Fig. 7). We then perform the same set of simulations, but in a rotated setup (Fig. 8). We rotate the substrate and the flux by 45° with respect to the simulation lattice. As can be seen from Fig. 9, the β vs. α from the non-rotated substrate and 45° rotated substrate are clearly different. The difference between the two results can be used as an estimate of the amount of grid effect on column angle simulation.

One way to remove grid effect is to change the unit particle in the simulation. Off lattice should be free of grid effect; however this type of simulation consumes more computing resources. We mitigate this problem by creating a simulation where the particle is a congregate/cluster of cubes (Fig. 10). The cubes that constitute the cluster still are confined in a simple cubic lattice, however the cluster itself are not confined to any lattice arrangement. As can be seen from Fig. 6 and Fig. 11, simulation using cluster of cubes results in dramatic reduction of the grid effect. Besides removing grid effect, the cluster

simulation also provides additional evidence that the so called “grid effect” is indeed caused by the on-lattice stacking of the cubic particles. [Note that the use of spherical particle in a simulation by itself does not imply that there is no grid effect. Some simulation uses spheres as particles but the spheres still have to stack according to a certain lattice geometry (i.e. it is still an on-lattice simulation). In this case, grid effect exists.]

DISCUSSION AND CONCLUSION

We laid down two useful tests related to grid effect. The first test is to determine whether a given simulation suffers grid effect. The second test is for estimating the amount of error in a simulated quantity of interest (such as column angle) caused by grid effect. We tested our cubic lattice MC simulation for grid effect. Fan angle simulations were carried out at different orientations with respect to the lattice geometry. This test method offers easy and undisputable confirmation of the presence of grid effect because it is clear that ideally (i.e. in absence of grid effect) fan angle should remain the same.

Likewise, any other simulated quantity of interest should ideally remain the same independent of the lattice rotation. We used this fact as a method to estimate the amount of error introduced by grid effect in any simulated quantity of interest. In this paper, we use column angle as an example. Using the fact that column angle simulation outcome ideally should not be altered by lattice rotation, we propose that the amount of deviation from this ideal behavior can be estimated as the amount of error.

Grid effect is most serious when a simulation involves comparison between depositions at various flux angles. As can be seen in Fig. 1 and Fig. 3, grid effect creates large artificial changes in a quantity that is supposed to be constant with respect to flux angle. For on-lattice simulations at 0° or near 90° that do not involve comparison with the intermediate flux angles, grid effect is not a big concern. For example, fan structure of Si can be simulated quite nicely using an on-lattice simulation with the proper amount of surface diffusion⁸. The reason is because for 0° or 90° , the manifestation of grid effect can be

removed by using appropriate amount of surface diffusion. But one would not be able to remove the grid effect for all angles (including 45°) simultaneously with any amount of diffusion. For this reason, on-lattice simulation performed on full range of deposition angles (such as column angle or porosity simulation) will suffer from grid effect.

In summary, we demonstrated that the widely used method of on-lattice particle simulation in OAD suffers an anomalous anisotropic “grid effect”. The grid effect significantly modifies OAD simulation outcomes such as column angle and indirectly, porosity; thus this is not necessarily a small effect that can be ignored. This anomalous grid effect is not observed in a semi off-lattice simulation we constructed, thus further verifying that grid effect is caused by the fixed lattice arrangement.

ACKNOWLEDGEMENTS

This work has been supported in part by NSF NIRT 0506738 and NSF REU 0850934. Curtis F. Doiron is an REU student from University of Oklahoma.

APPENDIX: CALCULATION OF GROWTH ANGLE

In Fig. 4 (d), the growth parallel to the flux (\vec{g}_p) and the growth sideways with respect to the flux (\vec{g}_s) are given by

$$\vec{g}_s = a\vec{j}, \text{ and}$$

$$\vec{g}_p = a\vec{i} + a\vec{j}. \tag{A1}$$

We denote the resultant vector from addition of the two vectors above as \vec{g}_t ,

$$\vec{g}_t = a\vec{i} + 2a\vec{j} . \quad (\text{A2})$$

The magnitude of this vector is $|\vec{g}_t| = a\sqrt{1^2 + 2^2} = a\sqrt{5}$.

We denote the angle between the resultant vector and the flux direction as γ . This angle can be obtained by

$$\cos(\gamma) = \frac{\vec{g}_t \cdot \vec{f}}{|\vec{g}_t| |\vec{f}|} , \quad (\text{A3})$$

where \vec{f} is a unit vector parallel to the flux direction,

$$\vec{f} = \frac{-\vec{i} - \vec{j}}{\sqrt{2}} . \quad (\text{A4})$$

Inputting Eq. (A4) and (A2) into Eq. (A3), it can be shown that $\gamma = 18.4^\circ$.

REFERENCES

- ¹ P. Meakin, *Fractals, scaling and growth far from equilibrium* (Cambridge University Press, 1998).
- ² A. L. Barabási and H. E. Stanley, *Fractal concepts in surface growth* (Cambridge University Press, 1995).
- ³ A. Lakhtakia and R. Messier, *Sculptured thin films: Nanoengineered morphology and optics*, Vol. PM **143** (SPIE Press Monograph, 2005).
- ⁴ M. M. Hawkeye and M. J. Brett, *Journal of Vacuum Science & Technology A: Vacuum, Surfaces, and Films* **25**, 1317 (2007).
- ⁵ Nieuwenh.Jm and H. B. Haanstra, *Philips Technical Review* **27**, 87 (1966).

- 6 R. N. Tait, T. Smy, and M. J. Brett, Thin Solid Films **226**, 196-201 (1993).
- 7 B. Tanto, G. Ten Eyck, and T. M. Lu, Journal of Applied Physics **108**, 026107 (2010).
- 8 D.-X. Ye and T.-M. Lu, Physical Review B **76**, 235402 (2007).
- 9 T. Karabacak, J. P. Singh, Y. P. Zhao, G. C. Wang, and T. M. Lu, Physical Review B **68**, 125408 (2003).
- 10 D. Vick, T. Smy, and M. J. Brett, Journal of Materials Research **17**, 2904-2911 (2002).
- 11 S. Lichter and J. Chen, Physical review letters **56**, 1396-1399 (1986).
- 12 C. Patzig, T. Karabacak, B. Fuhrmann, and B. Rauschenbach, Journal of Applied Physics **104**, 4318 (2008).
- 13 T. Smy, D. Vick, M. J. Brett, S. K. Dew, A. T. Wu, J. C. Sit, and K. D. Harris, Journal of Vacuum Science & Technology A: Vacuum, Surfaces, and Films **18**, 2507 (2000).
- 14 Y. G. Yang, R. A. Johnson, and H. N. G. Wadley, Acta Materialia **45**, 1455-1468 (1997).
- 15 S. W. Levine and P. Clancy, Modelling and Simulation in Materials Science and Engineering **8**, 751 (2000).
- 16 G. A. Kimmel, Z. Dohnálek, K. P. Stevenson, R. S. Smith, and B. D. Kay, The Journal of Chemical Physics **114**, 5295 (2001).
- 17 P. Meakin and J. Krug, Physical Review A **46**, 3390-3399 (1992).
- 18 G. H. Gilmer, H. Huang, T. D. de la Rubia, J. Dalla Torre, and F. Baumann, Thin Solid Films **365**, 189-200 (2000).
- 19 M. Cetinkaya, N. Malvadkar, and M. C. Demirel, Journal of Polymer Science Part B: Polymer Physics **46**, 640-648 (2008).
- 20 V. P. Zhdanov, K. Rechendorff, M. B. Hovgaard, and F. Besenbacher, Journal of Physical Chemistry B **112**, 7267-7272 (2008).
- 21 J. Yu and J. G. Amar, Physical Review E **66**, 21603 (2002).
- 22 L. Dong, R. W. Smith, and D. J. Srolovitz, Journal of Applied Physics **80**, 5682-5690 (1996).

- ²³ P. I. Wang, O. Nalamasu, R. Ghoshal, R. Ghoshal, C. D. Schaper, A. Li, and T.-M. Lu, Journal of Vacuum Science & Technology B: Microelectronics and Nanometer Structures **26**, 244 (2008).

FIGURE CAPTIONS

FIG. 1: (Color online) (a) Cross sectional view of a line seed (yellow) with the length of the line going into the page. Flux of parallel beams of particles impinging at various configurations: (b), (c) and (d) perpendicular onto the line seed yield fan structures of the same size and shape.

FIG. 2: (Color online) Scanning electron microscope (SEM) of (a) cross-sectional view of nanoimprinted Polyset pillar seeds, (b) top view of the same seeds, (c) cross-sectional view of 45° Si deposition on the pillar seeds, and (d) 0° (normal) Si deposition on the pillar seeds. The fan angle ϕ is defined as the angle subtended by the fan. The fan angles obtained from the two samples are very close (both $\sim 47^\circ$).

FIG. 3: (Color online) Fan structures obtained by simulation of deposition on line seeds. The simulation is a three dimensional Monte Carlo (3D MC) simulation with $D = 100$. The deposition angles are 0° , 15° , 30° , 45° , 60° , and 75° , as shown by the dotted grey lines. In all simulation figures in this paper, the 0° deposition angle is defined as the vertical direction. Orange arrows indicate positions of line seeds (the length of the line goes into the page). The size of the seed is 25 particles. Red solid lines indicate the fan angles. The amounts of deposited materials at the various angles are not the same. The deposition thickness is adjusted in such a way that the global shadowing between adjacent fans either has not started or has just started.

FIG. 4: (Color online) Explanation of the large difference in fan angles for depositions at (a) $\alpha = 0^\circ$ and (c) $\alpha = 45^\circ$ in an on-lattice simulation. For 0° deposition, the growth rates are determined by the two possible sites for deposition as shown by the dotted cubes in (b). The growth rates perpendicular to the flux (dashed arrow) and parallel to the flux (solid arrow) are the same. Similarly the growth rates for 45°

deposition are determined by the two possible sites for deposition as shown by the dashed cube in (d). The growth rate parallel to the flux and sideways with respect to the flux are not the same. The symbols shown are the notations used in the Appendix.

FIG. 5: (Color online) Similar simulation to Fig. 3, except with diffusion $D = 100$.

FIG. 6: (Color online) Comparison of fan angles obtained at various deposition angles using two different types of simulation: cubic particle and cluster particle. Some representative simulation output images are shown in Fig. 3, Fig. 5 and Fig. 11.

FIG. 7: (Color online) Columnar structures obtained using 3D MC simulation on seeded and unseeded surfaces (the orange-colored structures in the figure). Diffusion is turned off in the simulation. The flux angles α are: (a) 5° , (b) 25° , (c) 45° , (d) 65° , and (e) 85° . The simulation output image is trimmed in order to save space. The pitch of the pillars array is 100 cubic lattices, while the height of the pillars is 60 cubic lattices.

FIG. 8: (Color online) Columnar structures obtained using 3D MC simulation on a 45° rotated setup. The substrate is as shown by the orange structure in figure (a). It is the same substrate as the one in Fig. 7 with the exception that it is rotated 45° . Diffusion is turned off in the simulation. The flux angles α are: (b) 5° , (c) 25° , (d) 45° , (e) 65° , and (f) 85° . The simulation output image is trimmed in order to save space.

FIG. 9: (Color online) Plot of column angle versus flux angle for the simulation performed on rotated setup and non-rotated setup (Fig. 7 and Fig. 8).

FIG. 10: (Color online) (a) Cubic particle used in our 3D MC simulation. (b) The modified particle for semi off-lattice simulation. The cluster particle consists of six cubic particles (or seven if the center hidden cubic particle is counted) aggregated together into a single cluster. The number of possible stacking sites is 30, as opposed to 6 for a single cubic particle.

FIG. 11: (Color online) Semi off-lattice simulation using cluster particle depicted in Fig. 10(b). There is no diffusion in the simulation. The size of the simulation is 300×300 cubic lattices. The fan structures shown are (a) 0° deposition and (b) 45° deposition onto line seeds (length of the line is into the page). The locations of the line seeds are as indicated by the yellow arrows.

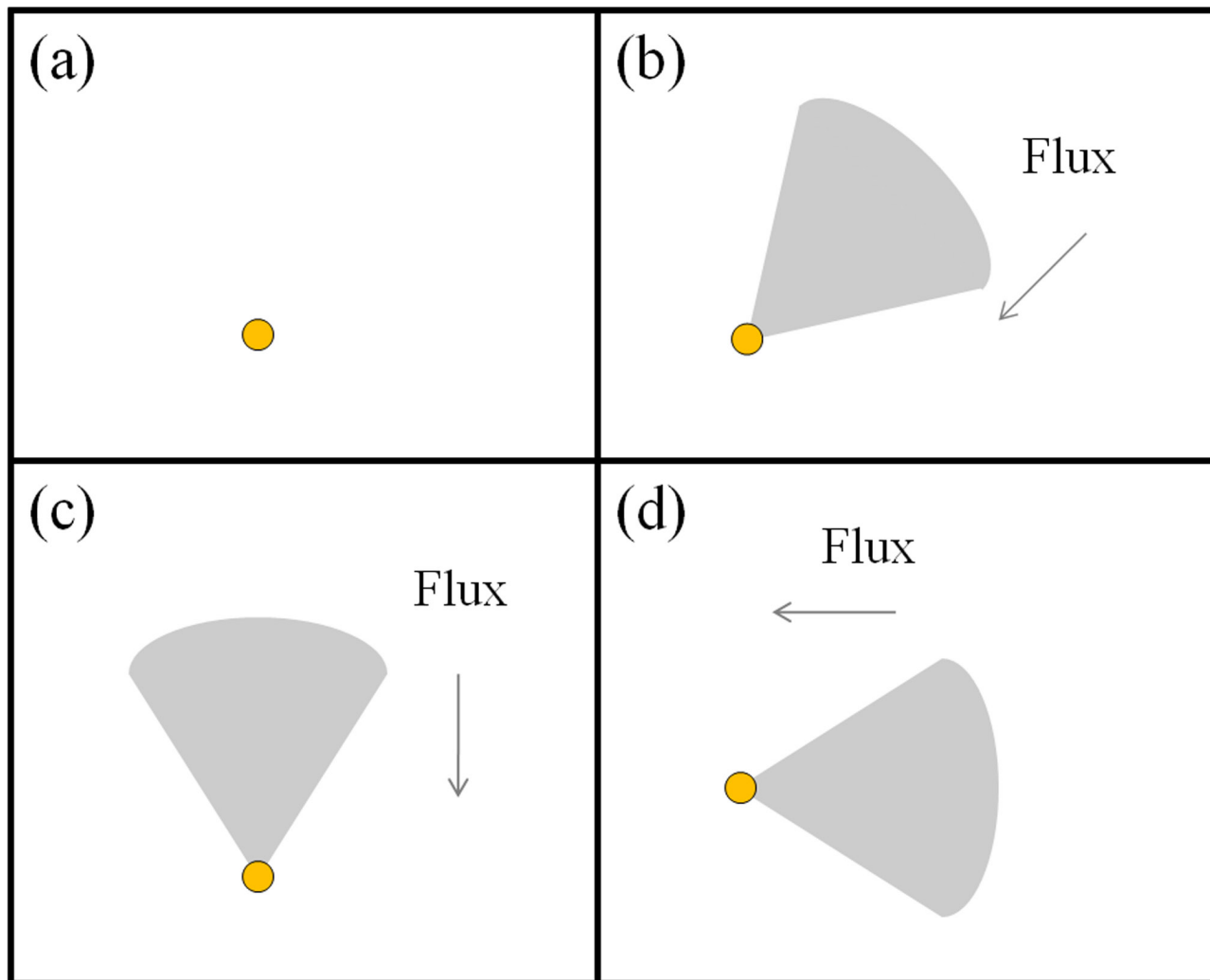


Figure 1 BW11202E 20DEC2010

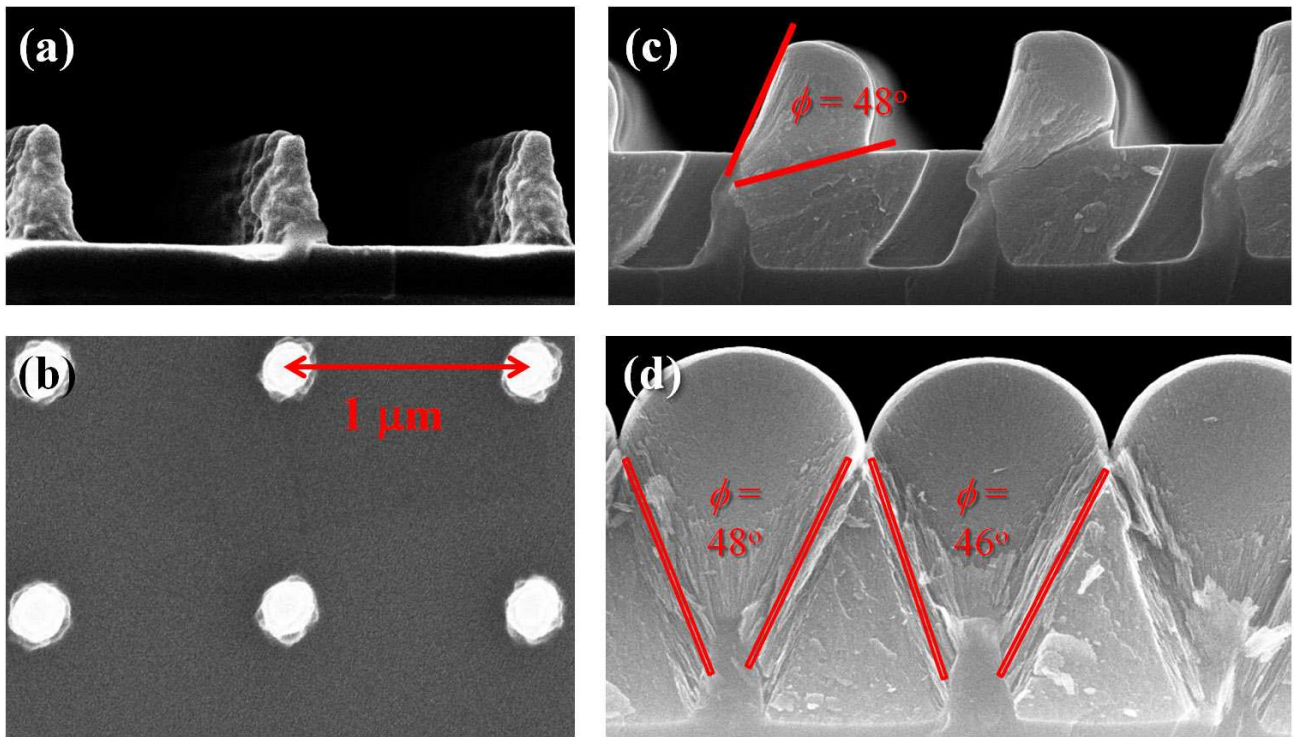


Figure 2

BW11202E

20DEC2010

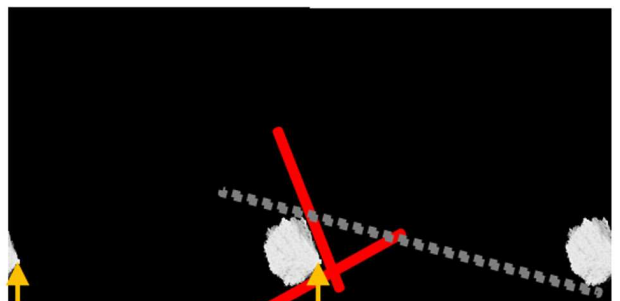
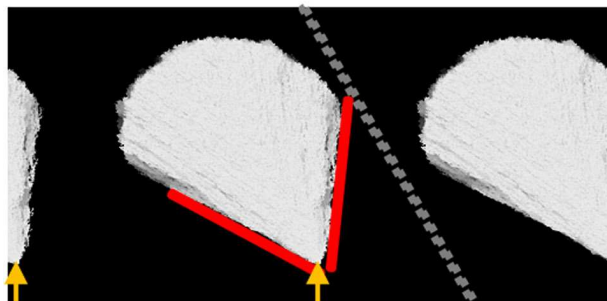
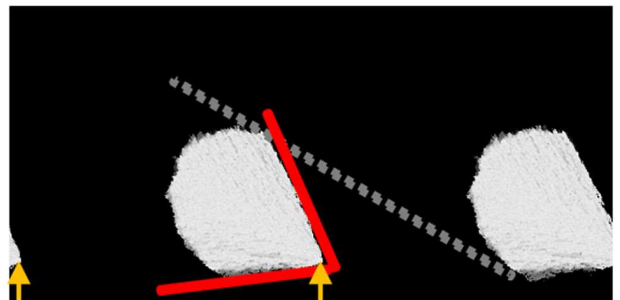
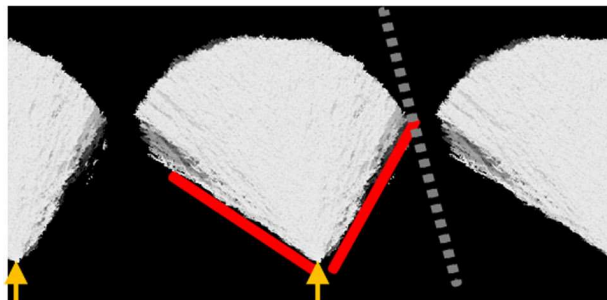
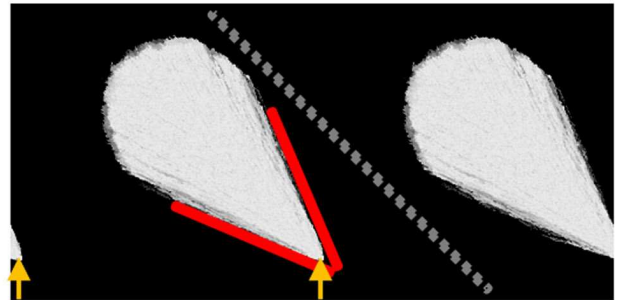
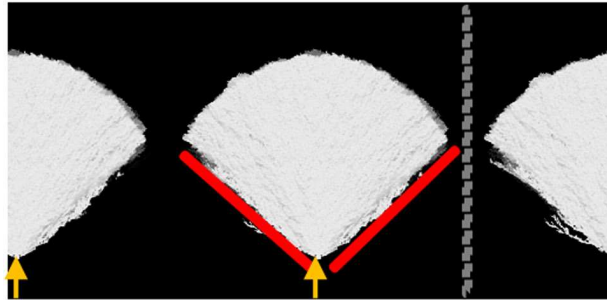


Figure 3 BW11202E 20DEC2010

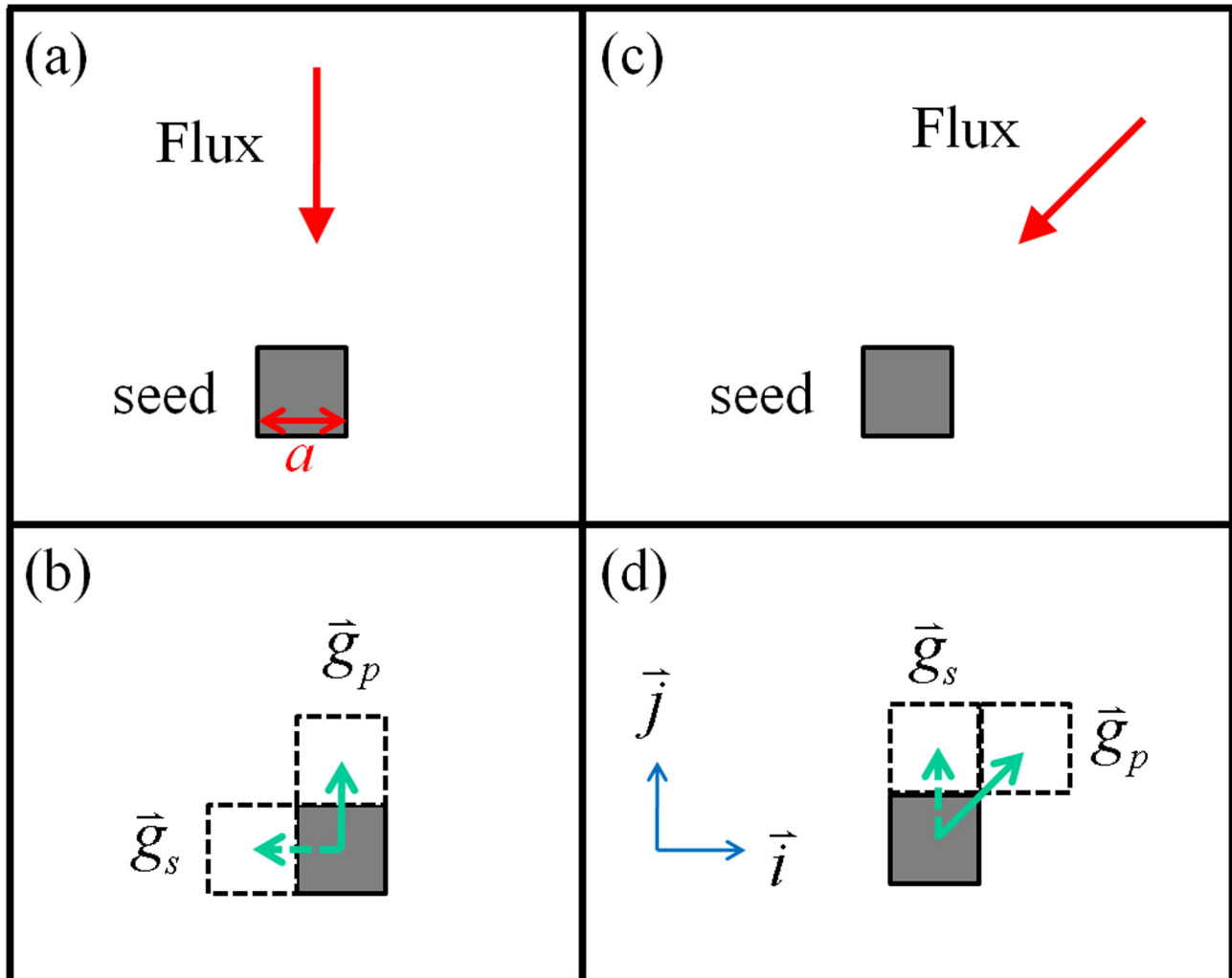


Figure 4

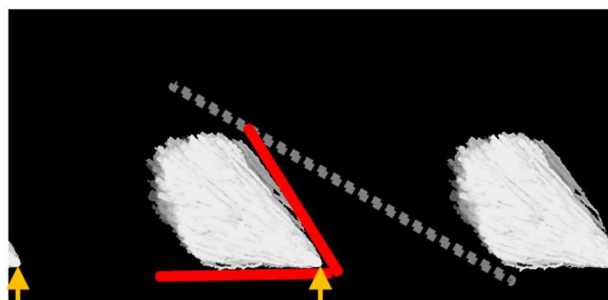
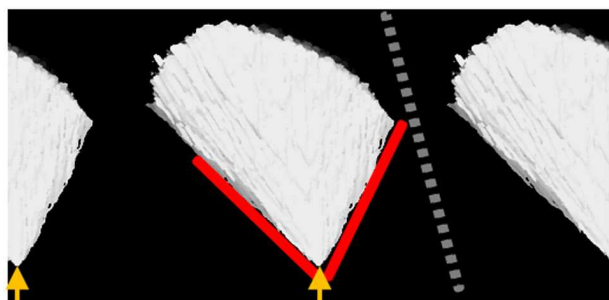
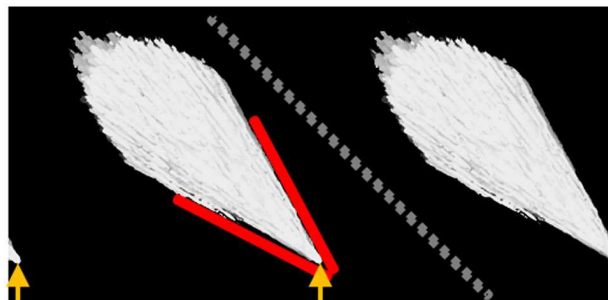
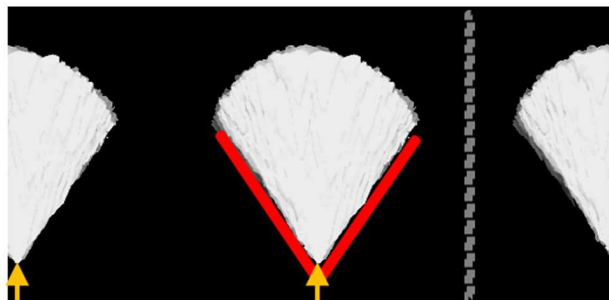


Figure 5

BW11202E

20DEC2010

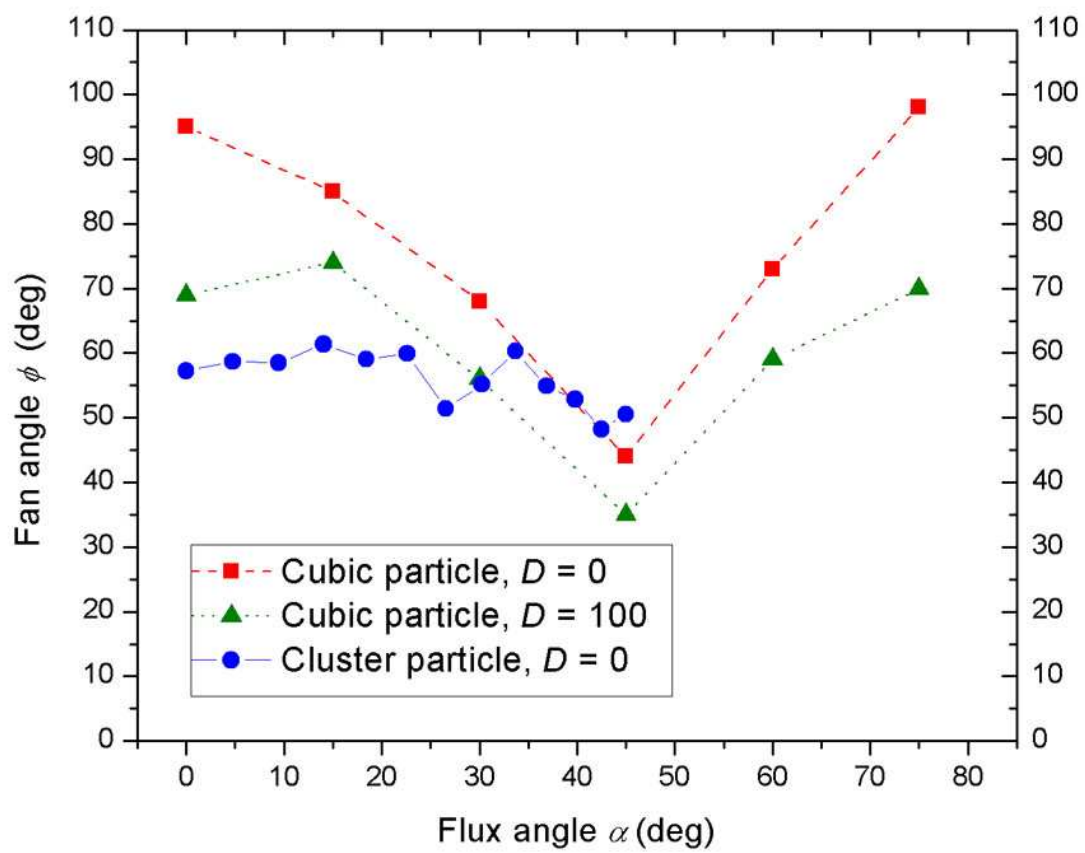


Figure 6

BW11202E

20DEC2010

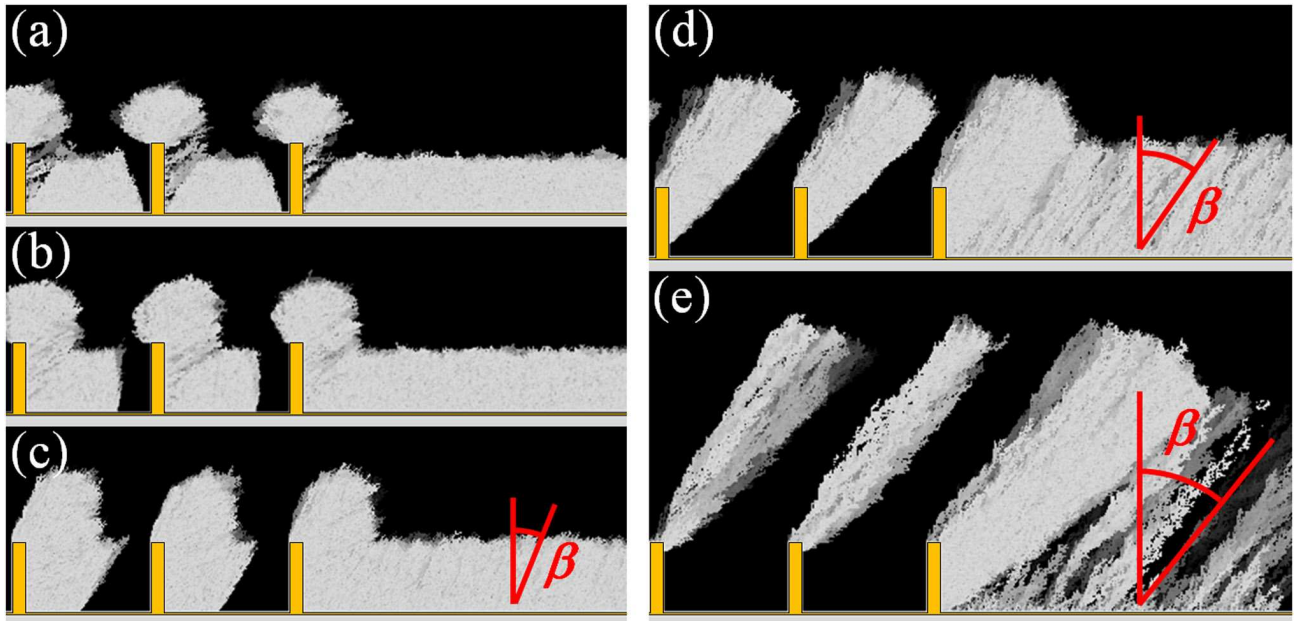


Figure 7 BW11202E 20DEC2010

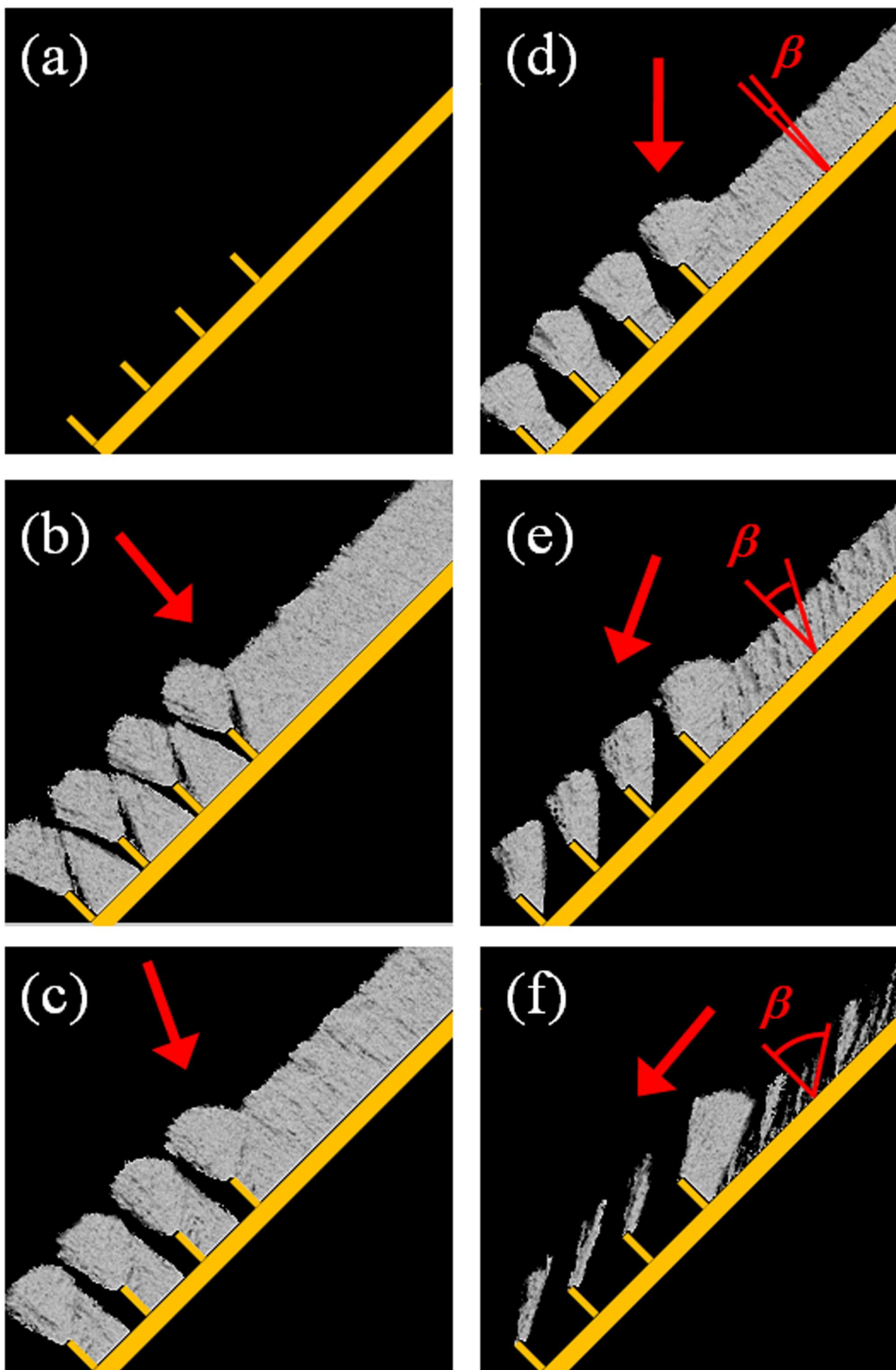


Figure 8

BW11202E

20DEC2010

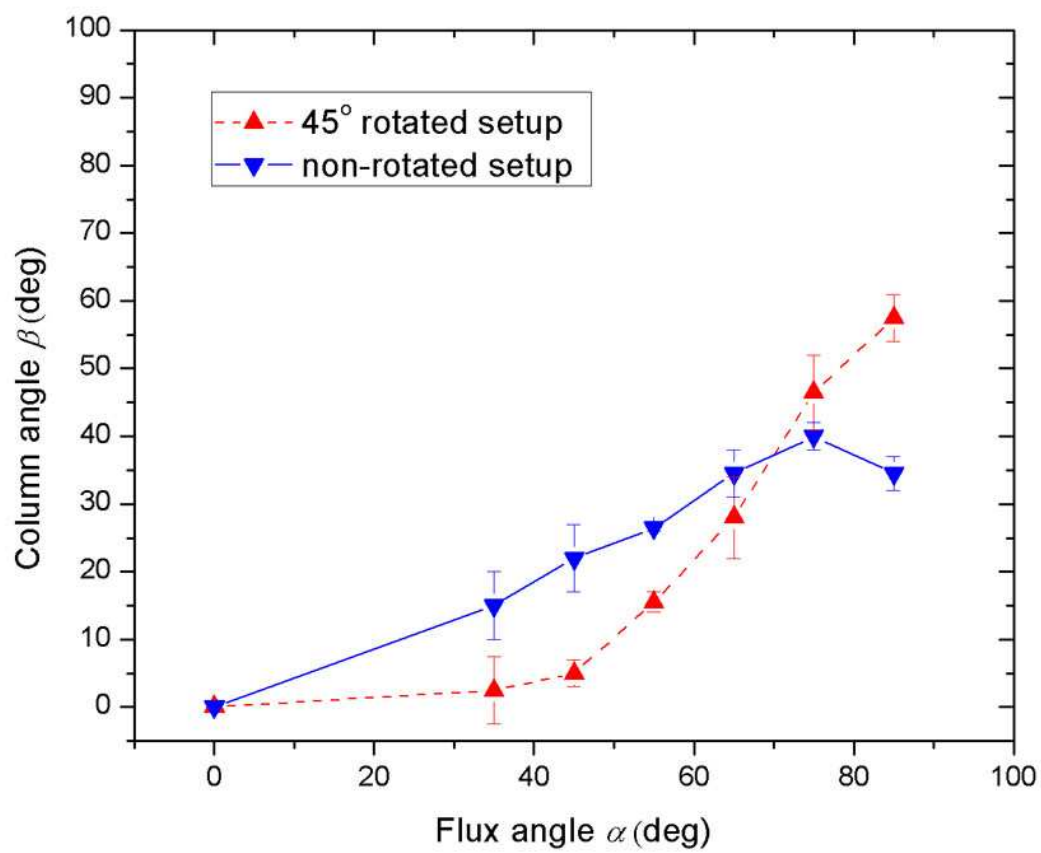


Figure 9

BW11202E

20DEC2010

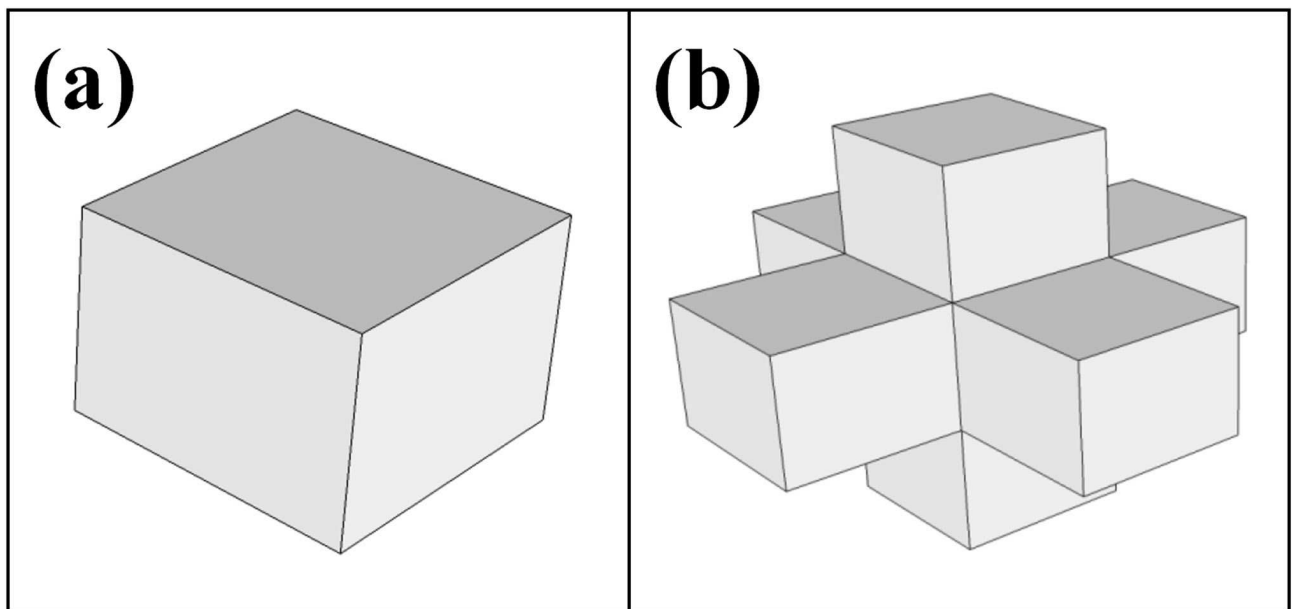


Figure 10 BW11202E 20DEC2010

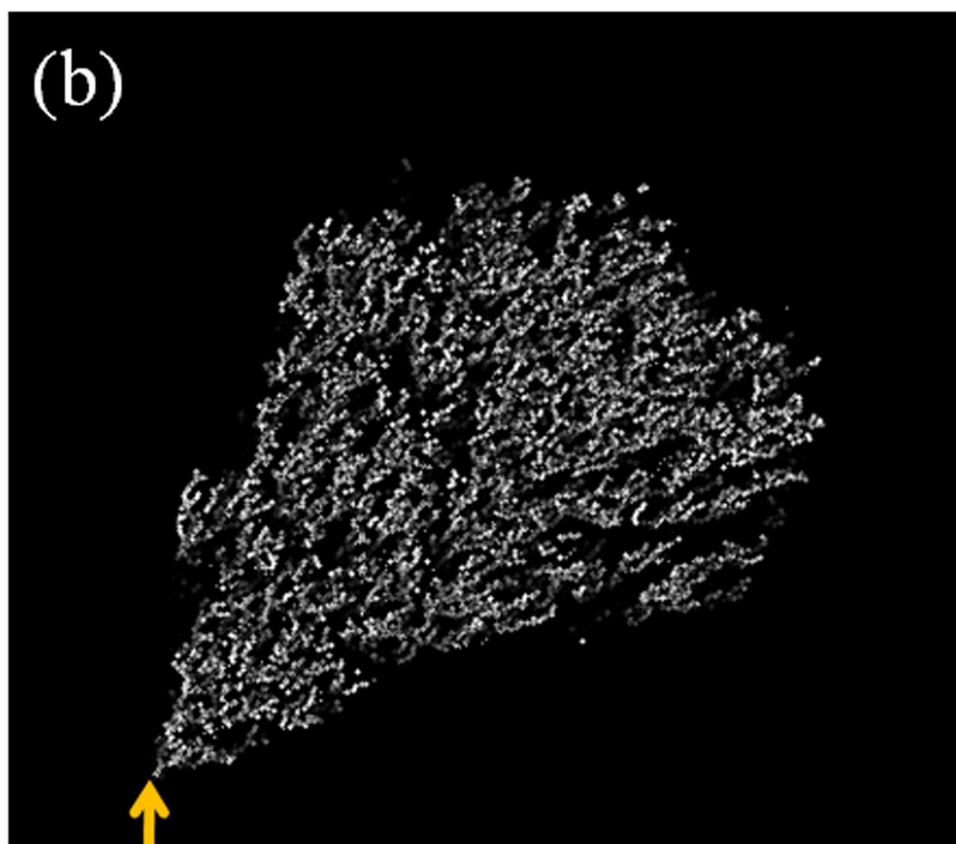
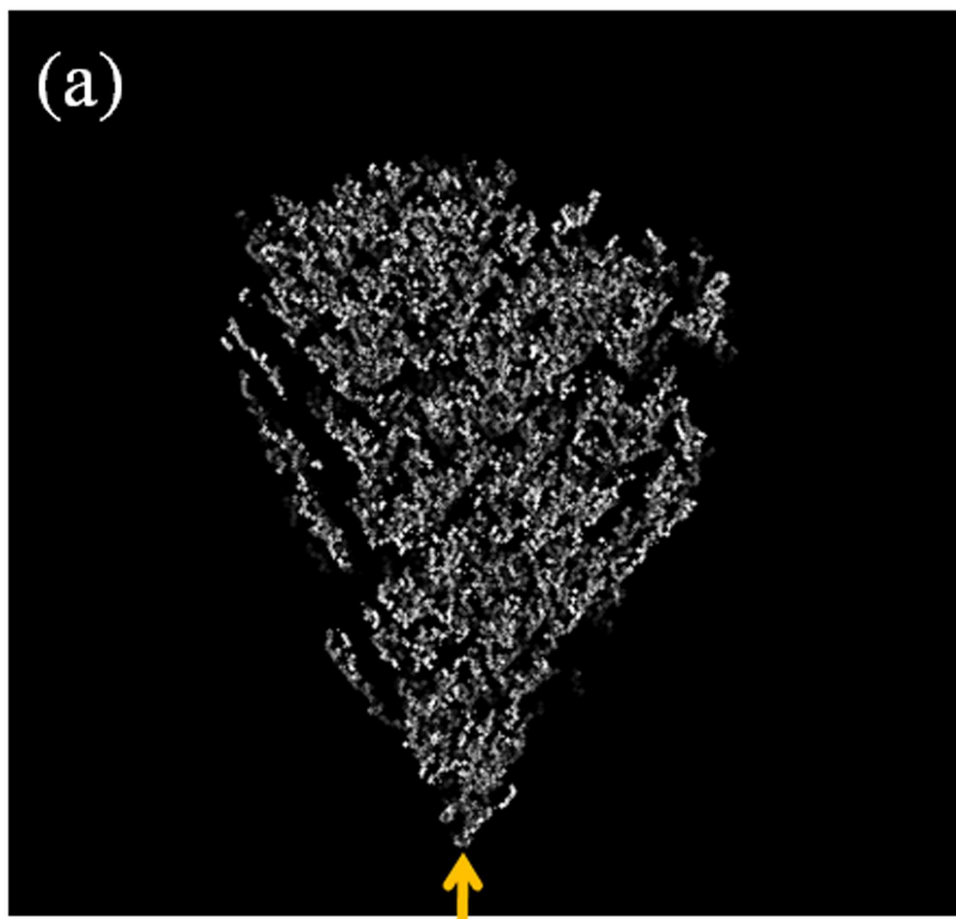


Figure 11 BW11202E 20DEC2010